Materials Transactions, Vol. 48, No. 7 (2007) pp. 1850 to 1854
Special Issue on Bulk Metallic Glasses —Selected Papers from the Fifth International Conference on Bulk Metallic Glasses (BMGV)
©2007 The Japan Institute of Metals

Corrosion Properties of Ca Based Bulk Metallic Glasses

James Dahlman[1,*1], Oleg N. Senkov[2,*2], James M. Scott[2] and Daniel B. Miracle[3]

[1]*SOCHE, Student Research Program, 3155 Research Blvd., Suite 204, Dayton, OH, 45420, USA*
[2]*UES, Inc., Materials and Processes Division, 4401 Dayton-Xenia Road, Dayton, OH, 45432, USA*
[3]*Air Force Research Laboratory, Materials and Manufacturing Directorate, Wright Patterson AFB, OH, 45433, USA*

The corrosion properties of ternary ($Ca_{65}Mg_{15}Zn_{20}$ and $Ca_{50}Mg_{20}Cu_{30}$), quaternary ($Ca_{55}Mg_{18}Zn_{11}Cu_{16}$), and quinternary ($Ca_{55}Mg_{15}Al_{10}Zn_{15}Cu_5$) amorphous alloys were evaluated using static aqueous submersion at room temperature. Ca-Mg-Zn and Ca-Mg-Cu alloy systems experienced destructive corrosion reactions. Ca-Mg-Zn-Cu and Ca-Mg-Zn-Cu-Al based amorphous alloys demonstrated positive corrosion properties, forming corrosion films up to 23 μm thick in the quaternary alloy and 11 μm thick in the quinternary composition. Corrosion products were evaluated using X-ray diffraction (XRD), X-ray Fluorescence (XRF), Scanning Electron Microscopy (SEM), and Energy Dispersive Spectroscopy (EDS). [doi:10.2320/matertrans.MJ200732]

(Received November 14, 2006; Accepted December 18, 2006; Published June 25, 2007)

Keywords: *metallic glass, corrosion, calcium, calcium alloy*

1. Introduction

Bulk amorphous metals are attractive materials for several reasons. An absence of microstructural features such as crystal planes, dislocations, grain and phase boundaries contribute to appealing mechanical properties such as high hardness and high specific strength. The amorphous structure can also result in attractive magnetic properties such as high magnetic permeability. Corrosion studies have also established amorphous metals as a group of materials with corrosion properties much more desirable than their crystalline counterparts. As a result, metallic glasses have found their way into common applications including golf club heads, magnetic security strips, step-down transformers and cell phone cases. Within the last 15 years, many successful steps have been made in both understanding the properties of amorphous metals and in processing bulk quantities efficiently.

Calcium based bulk metallic glasses constitute a new class of amorphous materials. The first successful synthesis of Ca-based bulk metallic glasses (Ca BMGs) produced $Ca_{57}Mg_{19}Cu_{24}$ and $Ca_{60}Mg_{20}Ag_{20}$ in amorphous cylinders with diameters up to 4 mm[1)] and $Ca_{60}Mg_{20}Ag_{10}Cu_{10}$ with a maximum diameter of 7 mm.[2)] Since then, additional work has provided specific criteria for selecting Ca BMG compositions[3–6)] and a number of Ca BMG's have been produced in Ca-Mg-Zn,[7–11)] Ca-Mg-Cu,[11,12)] Ca-Mg-Al[4,13)] and other systems.[4,13)] Significant interest and development in these materials has been catalyzed by properties that include low densities approaching $\sim$2.0 g/cm^3 and a low Young's modulus, near 20–35 GPa.[14)] However, crystalline Ca is extremely reactive, and studies evaluating the corrosion resistance of amorphous Ca-based alloys are required to explore what may be a limiting factor for practical applications of Ca BMGs.[15)]

The purpose of this report is to describe the stability of Ca BMGs in a static aqueous environment. The results from two ternary alloys ($Ca_{65}Mg_{15}Zn_{20}$ and $Ca_{50}Mg_{20}Cu_{30}$), one quaternary alloy ($Ca_{55}Mg_{18}Zn_{11}Cu_{16}$) and one quinternary alloy ($Ca_{55}Mg_{15}Al_{10}Zn_{15}Cu_5$) will be discussed. A uniform procedure for preparing Ca BMGs for corrosion analysis was developed and will be described. The discourse will assess the change in mass of each sample and attempt to identify the experimental reaction byproducts. The results of these trials will help guide further development of CaBMG corrosion resistance so that applications may take advantage of their attractive properties. Finally, a correlation between the chemical composition and the corrosion resistance of CaBMGs will be identified.

2. Experimental Procedures

Four alloys were chosen to assess the individual contributions from different alloying additions. Previous work established high glass forming ability (GFA) of Ca-Mg based BMGs.[6–12)] Zn and Cu were chosen both individually and alloyed together, in order to evaluate the corrosion resistance in the Ca-Mg system. Finally, Al was chosen to evaluate the corrosion effect of this protective oxide-forming element. Each composition was prepared with high purity elements (see Table 1). The mass of each individual component was calculated for a 15-gram sample, and was weighed to within one-tenth of a milligram. Once measured, the elements were mixed and induction melted in a water-cooled Cu hearth with a diameter of 31.75 mm under a positive pressure argon atmosphere. Once the alloy was successfully produced, it was placed in a vacuum desiccation chamber until it was ready to be cast. Total exposure time between melting and placement in the desiccator was limited to less than twenty minutes to minimize possible corrosion reactions between the specimen and the environment.

Table 1 Purity of elemental constituents.

Element	Ca	Mg	Zn	Cu	Al
Purity	99.5%	99.98%	99.99%	99.99%	99.9%

*[1]Undergraduate Student, Wright State University, Dayton, Ohio 45435, USA
*[2]Corresponding author, E-mail: oleg.senkov@wpafb.af.mil

Table 2 Alloy compositions sought to evaluate differences in corrosion resistance with different elements.

Composition (at%)	$Ca_{55}Mg_{18}Zn_{11}Cu_{16}$	$Ca_{65}Mg_{15}Zn_{20}$	$Ca_{50}Mg_{20}Cu_{30}$	$Ca_{55}Mg_{15}Al_{10}Zn_{15}Cu_5$^
Composition (mass%)	$Ca_{50}Mg_{10}Zn_{16}Cu_{23}$	$Ca_{61}Mg_8Zn_{31}$	$Ca_{46}Mg_{11}Cu_{43}$	$Ca_{53}Mg_9Al_6Zn_{24}Cu_8$
Theoretical Density* (g/cm^3)	2.31	2.05	2.45	2.16
Maximum amorphous Thickness (mm)	>10.0	6.0	8.0	6.0

*Theoretical density was calculated using the following equation:

$$\rho = \frac{100}{\sum_{i=1}^{n}\left(\frac{mass\%}{\rho}\right)_i}$$

^The alloy was first reported by F. Guo, J. Poon and G. Shiflet at DARPA SAM1 in 2005.

Approximately 5.0 grams of each alloy was induction remelted under a positive pressure argon gas in a quartz crucible with a 2 mm hole in the bottom and injected into a water-cooled Cu mold cavity with dimensions of 15 mm × 15 mm × 4 mm. Previous work demonstrated that these alloys have the maximum amorphous thicknesses well beyond 4 mm (see Table 2). Consequently it was assumed that the samples were amorphous throughout; although amorphicity of their surface layers was additionally verified by XRD.

To maintain a uniform surface with an easily measured surface area, each sample was first polished on 320 grit SiC paper, then on 600 SiC grit paper with water lubricant until a rectangular prism was produced. The samples were then briefly ground on 600 grit SiC paper without water to remove corrosion products from the surface. Once polishing was complete, each alloy underwent dimensional analysis with a pair of digital calipers accurate to within ±0.01 mm. Less than twenty minutes after polishing, the samples were placed in a vacuum desiccator until the corrosion testing began.

The experiment evaluated the corrosion resistance in a static aqueous environment with a timeframe of up to 2100 hours. One sample from each alloy was attached to a nylon string and clasp with a mass of 0.1710 g. The sample was then suspended in 150 mL of distilled water by attaching the clasp around a cylindrical piece of wood, and suspending the wood over the opening to a 250 mL beaker. An Al hook system was attached to a scale to measure the sample mass at selected times during the exposure. Sample weight change data points were collected while the sample was in distilled water.

After ~700 hours of exposure in water, the Ca-Mg-Cu alloy was completely decomposed into its corrosion by-product in the form of powder. After ~2100 hours, the Ca-Mg-Zn alloy also entirely decomposed into powder. These corrosion products were strained with filter paper for one hour, then heat treated at 100°C for seventy-two hours in order to remove the water from the powder. An X-ray diffractometer, Rigaku Rotaflex, using Cu K_α radiation was used to identify phases in each respective sample and to evaluate the sample surface amorphicity. A scanning electron microscope with an attached energy-dispersive spectrometer was used to analyze the microstructure and chemistry of the amorphous samples and corrosion products.

Powdered samples were prepared for SEM analysis by coating with carbon to ensure electrical conductivity across the entire sample. Solid amorphous samples with oxidized surfaces were cross-sectioned and cold mounted in epoxy. The surfaces were then mechanically polished, cleaned and the mounts were also carbon coated. Any heating during processing was minimized to avoid crystallization. SEM was performed at 15 keV, using both secondary electron and back-scatter electron imaging, and EDS analysis was conducted using an accelerated voltage of 25 kV to ensure data quality.

3. Results and Discussion

3.1 Corrosion and crystallization during the sample surface polishing

While in contact with water during polishing, the $Ca_{65}Mg_{15}Zn_{20}$ amorphous alloy was very reactive, bubbling violently. However, it showed an exceptionally low pitting frequency. The other alloys did not corrode as aggressively, but had pitting present over many of the large faces. XRD performed on 14 samples following the polishing procedure showed that the sample surface remained fully amorphous if water or oil were used as a coolant and a low polishing pressure was applied during the surface grinding and polishing (Fig. 1(a)). However, after dry polishing, without using water or oil, the surface layer of the amorphous samples was partially crystallized and corresponding XRD patterns showed crystalline peaks (Fig. 1(b)). The $Ca_{65}Mg_{15}Zn_{20}$ amorphous samples were most sensitive for crystallization as they had the lowest crystallization temperature of $T_x = 137°C$,[9] followed by, $Ca_{55}Mg_{15}Al_{10}Zn_{15}Cu_5$ ($T_x = 149°C$), $Ca_{55}Mg_{18}Zn_{11}Cu_{16}$ ($T_x = 166°C$)[11] and $Ca_{50}Mg_{20}Cu_{30}$ ($T_x = 169°C$).[12]

3.2 Corrosion in Water

The four amorphous alloys subjected to static aqueous environment underwent corrosive reactions. $Ca_{65}Mg_{15}Zn_{20}$ and $Ca_{50}Mg_{20}Cu_{30}$ both underwent corrosive reactions

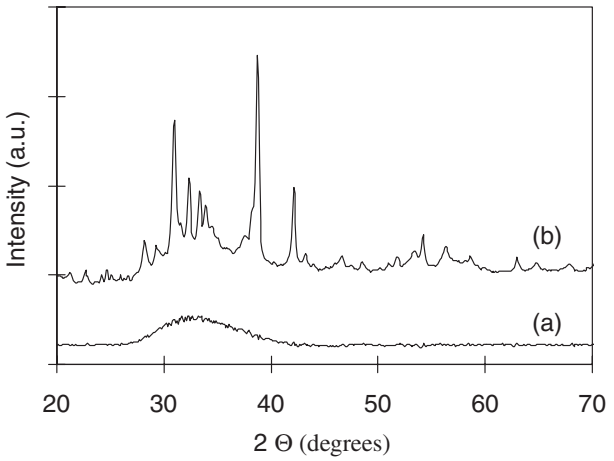

Fig. 1 X-ray diffraction patterns of $Ca_{50}Mg_{20}Cu_{30}$ amorphous plates after (a) grinding and polishing with cooling water and oil and (b) after dry grinding and polishing. A broad halo is seen in figure (a), indicating amorphicity at the surface of the sample polished with low pressure and low heat; while both the amorphous halo and crystalline peaks are seen in figure (b).

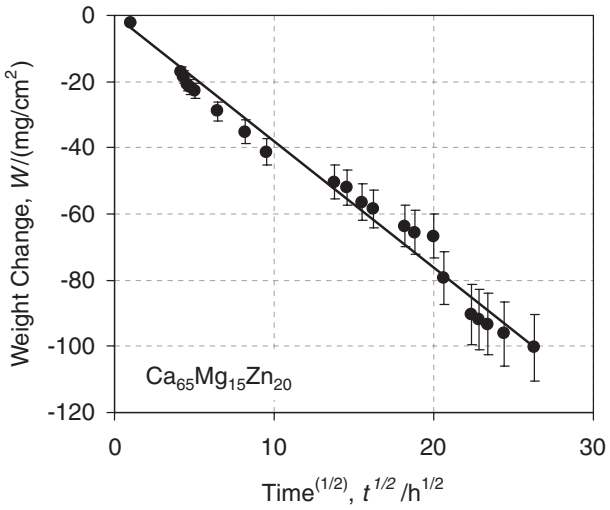

Fig. 2 Weight change per unit surface area of a ternary $Ca_{65}Mg_{15}Zn_{20}$ metal glass versus square root of holding time in distilled water. The weight loss can be fit by a parabolic time dependence, $W_1 = -a_1 t^{0.5}$, where $a_1 = 1.06 \times 10^{-3}$ mg/(cm^2 s$^{0.5}$) is a rate constant.

resulting in a net loss of mass from the samples due to spallation of the corrosion products. When placed in distilled water, an immediate reaction with the $Ca_{65}Mg_{15}Zn_{20}$ amorphous alloy took place. The surface area was quickly covered in bubbles stemming from a corrosion reaction. The corrosion reaction between $Ca_{65}Mg_{15}Zn_{20}$ and distilled water led to the formation of a non-protective compound on the sample surface, which spalled off and collected at the bottom of the beaker in a white and gray powder form. At one point during the experiment the spalled material blended with the distilled water, creating an opaque environment. These unstable reaction products and the consequent loss in mass established $Ca_{65}Mg_{15}Zn_{20}$ unsuitable for sustained exposure to aqueous environments.

The time dependence of the weight loss per unit surface area of a $Ca_{65}Mg_{15}Zn_{20}$ amorphous sample during reaction with distilled water is shown in Fig. 2. The weight continuously decreases with time and after ~700 hour holding in water, the sample loses about 65% of its mass. The experimental results also indicate that the weight loss per unit area, W, can be described by a parabolic dependence on the holding time, t, with a rate constant $a_1 = -1.06 \times 10^{-3}$ mg/(cm^2 s$^{0.5}$) and $b_1 = 0$:

$$W = at^{0.5} + b \quad (1)$$

X-ray analysis of the spalled corrosion powder product from the $Ca_{65}Mg_{15}Zn_{20}$ amorphous sample identified three primary phases, which were Calcium Hydroxide ($Ca(OH)_2$), Calcium Zinc Hydroxide Hydrate ($Ca[Zn(OH)_3]_2 \cdot H_2O$) and Calcium Zinc ($Ca_3Zn$). Supporting the XRD results, X-ray fluorescence of the powder indicated a major concentration of Ca and Zn, with Mg existing in only minor concentrations.

Corrosion behavior of the ternary $Ca_{50}Mg_{20}Cu_{30}$ glassy alloy is illustrated in Fig. 3 and it is considerably different from that of $Ca_{65}Mg_{15}Zn_{20}$. During the first 100 hours of distilled water exposure the $Ca_{50}Mg_{20}Cu_{30}$ amorphous alloy showed a very minor weight gain due to the creation of an oxide layer (see Fig. 3 enclosure). This increase in weight

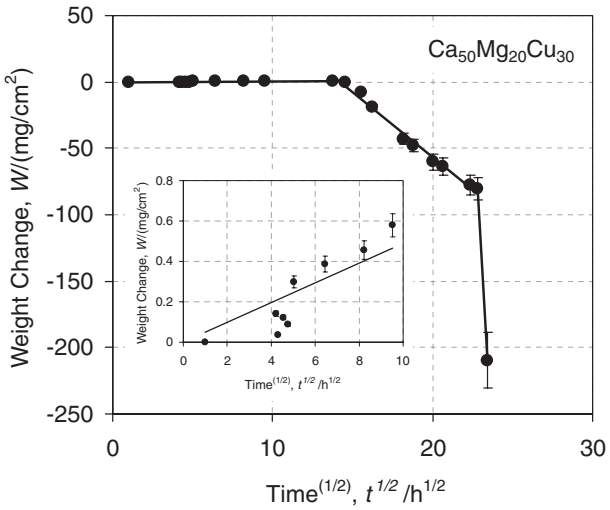

Fig. 3 Weight change per unit surface area of a ternary $Ca_{50}Mg_{20}Cu_{30}$ metal glass versus square root of holding time in distilled water. Insert shows behavior during the first 100 hours of holding in water.

can be described by a parabolic time dependence, Equation (1), with the rate constant $a_2 = 1.36 \times 10^{-5}$ mg/(cm^2 s$^{0.5}$) and $b_2 = 0$. However, after this point, the alloy started to lose weight and black spalled material appeared at the bottom of the beaker. After ~150 hours of the distilled water exposure, the non-protective reaction product and the corrosion layer visible on the specimen changed in color from black to a blend of gold and black, and a rapid decrease in mass was observed. This rapid decrease in the weight, within 150 to 500 hours of holding in water, can be described by Equation (1) with $a_3 = -2.73 \times 10^{-3}$ mg/(cm^2 s$^{0.5}$) and $b_3 = 140$ mg/cm^2. The heavy corrosion reaction was evidenced by a drastic change in amount of the surface area covered by gaseous bubbles. After about 550 hours of exposure, rapid drops in the sample weight occurred leading to complete decomposition of the sample (see Fig. 3).

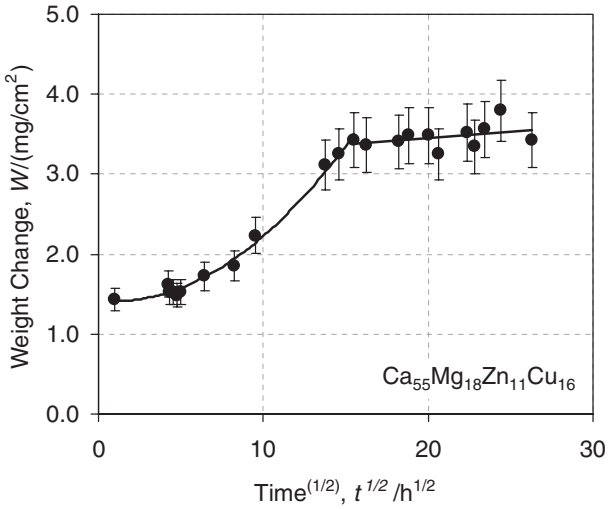

Fig. 4 Weight change per unit surface area of a $Ca_{55}Mg_{15}Zn_{11}Cu_{16}$ metal glass versus square root of holding time in distilled water.

X-ray diffraction of the spalled corrosion product from the $Ca_{50}Mg_{20}Cu_{30}$ amorphous sample showed the presence of two primary phases, Cu_2O and $Ca(OH)_2$, and several minor unidentified phases. X-ray fluorescence (XRF) chemical analysis supports the presence of these two major phases, indicating a strong concentration of Ca and Cu in the spalled corrosion product.

Contrasting the heavy corrosion of the pair of the ternary alloys, both the quaternary alloy ($Ca_{55}Mg_{18}Zn_{11}Cu_{16}$) and the quinternary alloy ($Ca_{55}Mg_{15}Al_{10}Zn_{15}Cu_5$) demonstrated much better corrosion behavior, steadily gaining weight. The quaternary $Ca_{55}Mg_{18}Zn_{11}Cu_{16}$ alloy gained mass at a linear rate for the first 250 hours (Fig. 4). The time dependence of the weight gain can be described by a linear equation:

$$W = ct + d \tag{2}$$

where $c = 2.45 \times 10^{-6}\,\mathrm{mg/(cm^2\,s)}$ is the linear oxidation rate and $d = 1.36\,\mathrm{mg/cm^2}$. Bubbles were present on the blackened specimen throughout the testing. After ~250 hours, a small amount of black spalled material formed on the bottom of the glass beaker. Once the spalled material was observed, the corrosion behavior of $Ca_{55}Mg_{18}Zn_{11}Cu_{16}$ changed from linear to parabolic (Fig. 4), which can be described by Equation (1) with $a_4 = 4.81 \times 10^{-6}\,\mathrm{mg/(cm^2\,s^{0.5})}$ and $b_4 = 3.1\,\mathrm{mg/cm^2}$. After ~700 hours, the sample had increased 17.4 milligrams, or 1.636%. This large change in mass was verified by SEM analysis indicating an oxide film with a thickness of ~18–23 μm after corrosion in water for ~2100 hours (Fig. 5). The film appeared to consist of three layers, with the majority of the structural defects occurring in the second layer. The bright region at the bottom of this picture represents an image of a non-oxidized sample, above which three oxide layers are seen, which are identified by different gray levels. The first oxide layer, which is adjacent to the non-oxidized sample region, is approximately 1–1.5 μm thick and dark-gray. It does not have any visible defects, except small cracks propagated from the second layer. The intermediate layer is much thicker, with the thickness of about 8–12 μm. It has a lighter contrast and shows a high crack frequency, with open cracks perpendicular to the sample surface. The third (external) layer is also thick, with the thicknesses varying from 5 to 10 μm. It has the darkest contrast and an uneven external surface. The different contrasts of the oxide layers in the backscatter electron imaging mode indicates different chemistry of these layers. Darker contrast indicates higher concentration of lighter elements. EDS analysis of the oxide layers in the $Ca_{55}Mg_{18}Zn_{11}Cu_{16}$ amorphous alloy showed a large presence of Ca, Mg and O in the outermost layer. This analysis also indicated that the first thin oxide layer mainly contains Ca, Zn and O, while the middle layer contains an increased concentration of Cu, Ca and O.

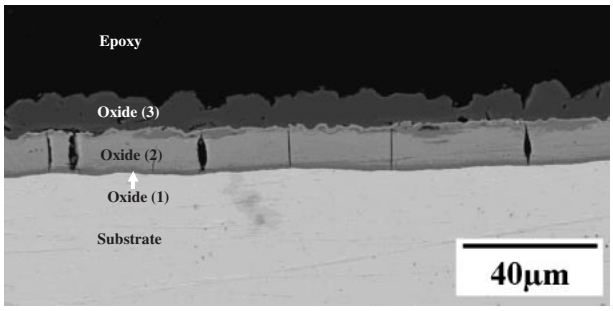

Fig. 5 SEM backscatter image of a near surface region of a $Ca_{55}Mg_{18}Zn_{11}Cu_{16}$ amorphous sample after corrosion in distilled water for 2100 hours. The bright region at the bottom represents an image of a non-oxidized sample, above which three oxide layers are seen, which are identified by different gray levels.

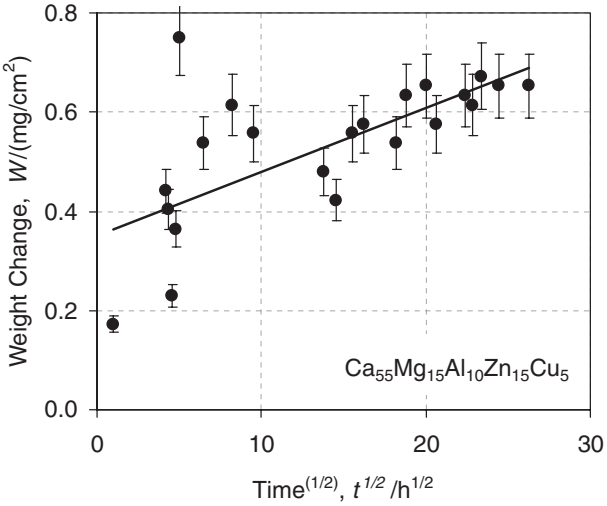

Fig. 6 Weight change per unit surface area of a $Ca_{55}Mg_{15}Al_{10}Zn_{15}Cu_5$ metal glass versus square root of holding time in distilled water.

The $Ca_{55}Mg_{15}Al_{10}Zn_{15}Cu_5$ amorphous alloy developed a very stable oxide layer during water exposure. Bubbles indicating the presence of a reaction were present throughout the experiment. The oxidation followed a parabolic dependence on oxidation time after some period of instability at the beginning of the experiment (Fig. 6). During the stable regime, the weight gain can be described by equation (1), with the parabolic rate $a_5 = 3.58 \times 10^{-6}\,\mathrm{mg/(cm^2\,s^{0.5})}$ and $b_5 = 0.35\,\mathrm{mg/cm^2}$. After holding in water for ~2100 hours, this amorphous alloy became very fragile and required careful handling to avoid breaking apart.

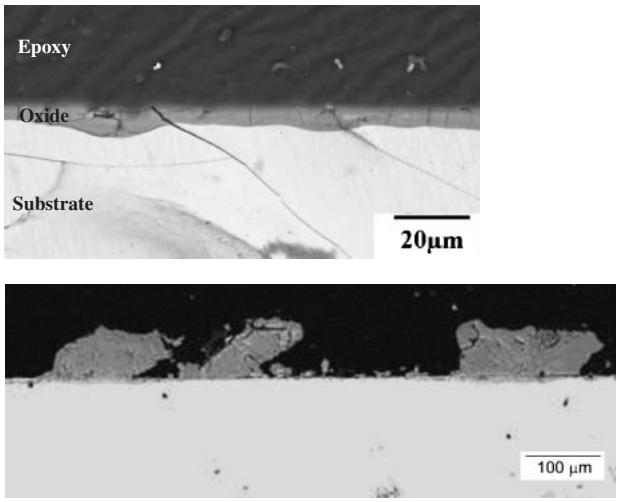

Fig. 7 SEM backscatter images of a near surface region of a $Ca_{55}Mg_{15}Al_{10}Zn_{15}Cu_5$ amorphous sample after corrosion in distilled water for 2100 hours. (a) A stable, even oxide layer ~7–11 μm. Cracks from corrosion do not propagate through the substrate. Cracks due to handling of brittle post-submersion alloy do propagate through the substrate. (b) Large globular oxide mounds up to 75 μm thick attached to the first oxide layer.

SEM analysis of the $Ca_{55}Mg_{15}Al_{10}Zn_{15}Cu_5$ amorphous alloy showed a double oxide layer. The first oxide layer, adjacent to the substrate, had an even thickness of about 7–11 μm along the entirety of the sample (Fig. 7(a)). Cracks perpetrated this oxide layer frequently. Many cracks, which are generally perpendicular to the sample surface, do not propagate inside the substrate. However, there are also a number of cracks which go through the oxide layer and the substrate. These latter cracks were probably formed during the sample handling supporting high fragility of the specimen after the distilled water corrosion testing. Finally, large globular mounds up to 75 μm thick were found attached to the first oxide layer (Fig. 7(b)). EDS showed the mounds to have a different chemical composition than the first oxide layer, with large amounts of Ca, Mg, Zn, and O in the globular formation. The analysis also indicated a strong presence of Ca, Mg, Zn, Cu, O and Al in the first oxide layer.

4. Summary and Conclusions

Ca-Mg-Zn and Ca-Mg-Cu bulk amorphous alloys demonstrated good glass forming ability and relatively low densities, but poor corrosion properties. During holding in distilled water, the $Ca_{65}Mg_{15}Zn_{20}$ alloy decomposed into a multiphase powder, with three primary phases; $Ca(OH)_2$, Ca_3Zn and $Ca[Zn(OH)_3]_2 \cdot H_2O$.

The $Ca_{50}Mg_{20}Cu_{30}$ amorphous alloy, during holding in distilled water for the first 100 hours, appeared to be stable and showed a very small increase in weight due to formation of a hydroxide layer. However, it decomposed rapidly into two major phases; Cu_2O and $Ca(OH)_2$, during the final 400 hours.

The $Ca_{55}Mg_{18}Zn_{11}Cu_{16}$ amorphous alloy was rather corrosion resistant in the aqueous environment. It gained mass, due to oxidation, at a linear rate for the first 250 hours and at a parabolic rate after that. The oxide film consisted of 3 distinctive layers and, after ~2100 hour exposure in distilled water, was ~18–23 μm thick, contributing to a gain in mass of 1.64%. However, the outermost oxide layer was subject to spallation. For this reason, further studies over longer time intervals should be included in order to evaluate the long-term stability of the oxide layer in this amorphous alloy.

Adding Al to form the $Ca_{55}Mg_{15}Al_{10}Zn_{15}Cu_5$ bulk amorphous alloy enhanced the stability of the oxide layer, which formed corrosion layers up to ~10 μm thick, and increased oxidation resistance. Adding Al also decreased the density of the alloy, making it very attractive for lightweight structures. However, after long time exposure in water this alloy became very fragile and broke easily under light pressure.

Acknowledgements

Discussions with William Rillo are greatly appreciated. Support for this research was provided by the United State Air Force Research Laboratory, on-site contract No. FA8650-04-D-5233, and by the Defense Advanced Research Project Agency (Dr. L. Christodoulou, Program Manager).

REFERENCES

1) K. Amiya and A. Inoue: Mater. Trans. **43** (2002) 81–84.
2) K. Amiya and A. Inoue: Mater. Trans. **43** (2002) 2578–2581.
3) O. N. Senkov and J. M. Scott: *MRS Proceedings*, Vol. 806, (Mater. Res. Soc., Warrendale, PA, 2003) pp. 145–150.
4) O. N. Senkov and J. M. Scott: Scripta Mater. **50** (2004) 449–452.
5) O. N. Senkov, D. B. Miracle and H. M. Mullens: J. Appl. Phys. **97** (2005) 103502-1-7.
6) S. Gorsse, G. Orveillon, O. N. Senkov and D. B. Miracle: Phys. Rev. B **73** (2006) 224202.
7) O. N. Senkov and J. M. Scott: Materials Letters **58** (2004) 1375–1378.
8) E. S. Park and D. H. Kim: J. Mater. Res. **19** (2004) 685–688.
9) O. N. Senkov and J. M. Scott: J. Non-Cryst. Solids **351** (2005) 3087–3094.
10) E. S. Park, W. T. Kim and D. H. Kim: Mater. Sci. Forum **475–479** (2005) 3415–3418.
11) O. N. Senkov, D. B. Miracle and J. M. Scott: Intermetallics **14** (2006) 1055–1060.
12) O. N. Senkov, J. M. Scott and D. B. Miracle: J. Alloys & Comp. **324** (2006) 394–399.
13) F. Q. Guo, S. J. Poon and G. J. Shiflet: Appl. Phys. Lett. **84** (2004) 37–39.
14) V. Keppens, Z. Zhang, O. N. Senkov and D. B. Miracle: Phil. Mag. **87** (2007) 503–508.
15) M. L. Morrison, R. A. Buchanan, O. N. Senkov, D. B. Miracle and P. K. Liaw: Metall. Mater. Trans. A **37** (2006) 1239–1245.